INDIAN JOURNAL OF SCIENCE AND TECHNOLOGY

*Corresponding author.

Tel: +91-9566406224
arantzajen1997@gmail.com

Stationary solutions, critical mass, Tadpole orbits in the circular restricted three-body problem with the more massive primary as an oblate spheroid

A Arantza Jency[1]*, Ram Krishan Sharma[1], Gagandeep Singh[1]

1 Department of Aerospace Engineering, Karunya Institute of Technology and Sciences, Coimbatore, 641114, Tamil Nadu, India. Tel.: +91-9566406224

Abstract

Background: The location and stability of the equilibrium points are studied for the Planar Circular Restricted Three-Body Problem where the more massive primary is an oblate spheroid. **Methods:** The mean motion of the equations of motion is formulated from the secular perturbations as derived by[1] and used in[2–4]. The singularities of the equations of motion are found for locating the equilibrium points. Their stability is analysed using the linearized variational equations of motion at the equilibrium points. **Findings:** As the effect of oblateness in the mean motion expression increases, the location and stability of the equilibrium points are affected by the oblateness of the more massive primary. It is interesting to note that all the three collinear points move towards the more massive primary with oblateness. It is a new result. Among the shifts in the locations of the five equilibrium points, the y–location of the triangular equilibrium points relocate the most. It is very interesting to note that the eccentricities (e) of the orbits around L_1 and L_3 increase, while it decreases around L_2 with the addition of oblateness with the new mean motion. The decrease in e is significant in Saturn-Mimas system from 0.95036 to 0.87558. Similarly, the value of the critical mass ratio μ_c, which sets the limit for the linear stability of the triangular points, further reduces significantly from $0.285\ldots A_1\ to\ 0.365\ldots A_1$ with the new mean motion. The mean motion s_z in the z-direction increases significantly with the new mean motion from $9A_1/4$ to $9A_1/2$.

Keywords: Circular Restricted Three-Body Problem (CRTBP); oblateness; mean motion; equilibrium points; critical mass ratio; tadpole orbits

1 Introduction

The restricted three-body problem (RTBP) has played an essential role in many different areas of dynamical astronomy and this will continue to do so. The modern applications to space mechanics are more powerful if not more numerous than the classical applications. The implications of the restricted problem for cosmology and

stellar dynamics are also numerous. Consider the famous classical three-body problem, the Sun-Earth combination and the determination of the motion of Moon. We might think of the two large bodies, the Sun and the Earth, which move around their centre of mass in approximate circles in their gravitational field and a third body, the Moon, moves on an approximate ellipse. This configuration is stationary in a sense, since no collisions take place. This is also true for the motions of a Trojan asteroid under the continued influence of Sun and Jupiter. On the other hand, one of the central problems in space science is to create artificial bodies. As such the study of the restricted three-body problem remained of utmost interest for many mathematicians and astronomers direct from Newton to Lagrange in the early days of its inception. In recent years, with the launching of artificial satellites in the Earth-Moon system and in the solar system, the applications of the restricted three-body problem to the celestial mechanics form the basis of some lunar and planetary theories. Euler was the first to contribute towards the restricted three-body problem in 1772 in connection with the lunar theories. Beginning with Euler and Lagrange in 1772, the theory of restricted three-body problem goes through Jacobi in 1836, Hill in1878, Brown in1896 and continue with Poincare in 1892, Levi-Civita in1904 and Birkoff in1915 and many more modern mathematicians and astronomers.

RTBP possesses five points of libration called equilibrium or Lagrangian points. Three collinear equilibrium points L_1, L_2 and L_3 lying on the line joining the two massive bodies are unstable in the Lyapunov sense, while two equilateral positions L_4 and L_5 are linearly stable for mass ratios $\mu < \mu_0 = 0.03852\ldots$ The locations of the equilibrium points in the restricted three-body problem by assuming both the primaries as oblate spheroids with their equatorial planes coincident with the plane of motion was calculated in [5]. In [6] the location of the collinear points in the same problem was studied numerically for some systems of astronomical interest. These equilibria were shown to be unstable in general, though the existence of conditional infinitesimal (linearized) periodic orbits around them was established. However, the secular effect of oblateness of the primaries on the motion of the primaries was not included. The oblateness of only the more massive primary was considered and the secular effect of oblateness[7] on the mean motion of the primaries was included in[8–12]. In[8,9], the critical mass value μ_c was found to decrease with oblateness. In[8,10], a numerical investigation of the locations of the five equilibrium points was made for some systems of astronomical interest. Periodic solutions of the linearized equations of motion around the five equilibrium points were studied. The angular frequency in the z-direction (s_z) was found to be more than the mean motion n. In[11] it was established that the oblateness induces a one-to-one commensurability at the exterior point L_3 and at the interior point L_2 for $0 \leq \mu \leq \frac{1}{2}$ and at L_1 no such commensurability exists. Series expansions were found for the long-periodic (S_4) short-periodic (S_5) orbits. s_4 was found to increase and s_5 was found to decrease with oblateness. A number of research publications were generated in RTBP by various authors by considering the more massive or smaller primary or both primaries as oblate spheroids with their equatorial planes coincident with the plane of motion. Some of the relevant publications are documented in[12–32].

In this paper we have included the secular effects of oblateness on the mean anomaly, argument of perigee and right ascension of ascending node[1]. We have obtained a new expression for mean motion of the primaries. We have utilized the new mean motion to study the above problem. We have calculated the locations of the equilibrium points and studied the stability of the equilibrium points using linearized equations of motion. Some interesting conclusions are drawn.

The collinear points and the y-coordinate of the triangular equilibrium points shift nearer to the origin due to the new mean motion. But, the x-coordinate of the triangular points does not show a change due to the variation in the mean motion till linear terms of oblateness. As opposed to an increase in the eccentricity of the periodic orbits around the collinear points reported when the previous mean motion was used, the eccentricity at the collinear point L_2 decreases. The eccentricities of the orbits at the other equilibrium points increased earlier with oblateness and it increases further with the new mean motion. As the mean motion value increases, the critical mass value (μ_c) shows further decrease from the critical mass value (μ_0) of the unperturbed case. Both the angular frequencies of the triangular points increase until μ becomes 0.0266053866. The value of mean motion at the triangular points in the z-direction shows further increase with the new mean motion.

The equations of motion, force function for the problem and the mean motion expression are defined (sections 1 and 2). The equilibrium points are located using the condition that the first derivative of the force function will equate to zero at these points (Section 3). The stability of the collinear equilibrium points are studied (Section 4.1). The critical mass ratio for the stability of the triangular equilibrium points is derived (Section 4.2). Also, the tadpole orbits around the triangular equilibrium points are studied (Section 5).

2 Equations of Motion

The problem is defined in the non-dimensional synodic coordinate frame as given by [Figure 1]. The barycentre of the primaries mark the origin of the system which rotates about the z-axis (perpendicular to the plane of motion of primaries). The mass ratio μ is the ratio of the mass of less massive primary m_2 to the sum of the masses of the primaries $m_1 + m_2$ which is unity in the non-dimensional system. Point P represents the point mass (with infinitesimal mass).

The equations of motion in terms of the dimensionless synodic frame is given by Equations (1)[10,33]. The force function Ω[8,10] in the equations is given by Equation (2). The oblateness of the more massive primary $A_1 = (R_E{}^2 - R_P{}^2)/5R^2$, R_E and R_P are equatorial and polar radii, respectively, and R is the distance between the primaries, affects the force function (2) of the system.

$$x'' - 2ny' = \Omega_x,$$
$$y'' + 2nx' = \Omega_y,$$

(1)

$$\Omega = \frac{n^2}{2}\left((1-\mu)r_1^2 + \mu r_2^2\right) + \left[\frac{1-\mu}{r_1} + \frac{\mu}{r_2} + \frac{(1-\mu)A_1}{2r_1^3}\right].$$

(2)

$$\Omega_x = \frac{\partial \Omega}{\partial x} = n^2 x - \frac{(1-\mu)(x-\mu)}{r_1^3} - \frac{\mu(x+1-\mu)}{r_2^3} - \frac{3A_1(x-\mu)(1-\mu)}{2r_1^5},$$

$$\Omega_y = \frac{\partial \Omega}{\partial y} = y\left[n^2 - \frac{(1-\mu)}{r_1^3} - \frac{\mu}{r_2^3} - \frac{3A_1}{2r_1^5}\right].$$

(3)

Referring [Figure 1], the distances r_1 and r_2 of P from the more massive and the smaller primaries are related to the distances x and y from the origin by

$$r_1^2 = (x-\mu)^2 + y^2,$$
$$r_2^2 = (x+1-\mu)^2 + y^2.$$

(3)

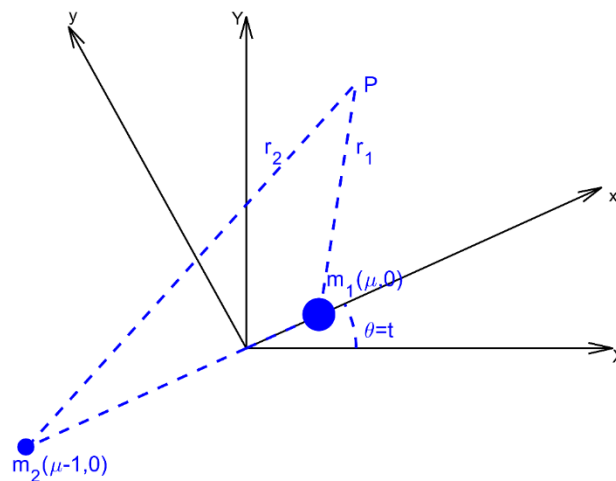**Fig 1.** Planar Restricted Three Body Problem in the fixed (sidereal) and rotating (synodic) coordinate system.

2.1 Mean Motion

The mean motion equation (Equation 5) for this study is derived using the effect of perturbation J_2, given by Equations (4)[34], on the three orbital elements – M_s - mean anomaly, ω_s - argument of perigee and Ω_s - right ascension of the ascending

node.

$$\frac{dM_s}{dt} = n\left[1 + \frac{3J_2}{2a^2\left(1-e^2\right)^{\frac{3}{2}}}\right], \frac{d\omega_s}{dt} = n\left[\frac{3J_2}{a^2\left(1-e^2\right)^2}\right], \frac{d\Omega_s}{dt} = n\left[\frac{-3J_2}{2a^2\left(1-e^2\right)^2}\right],\tag{4}$$

J_2 is Earth second zonal harmonic; a and e are semi-major axis and eccentricity, respectively.

The mean motion n is the summation of the changes in M_s, ω_s and Ω_s after one revolution[1]. Averaging the above equations for one revolution and summing them up, the mean motion expression after simplification is obtained, as in[1], given by

$$n = 1 + \frac{3A_1R^2}{2a^2\left[\left(1-e^2\right)Re\right]^2}\left(1+\sqrt{1-e^2}\right).$$

When the value of eccentricity e becomes zero and we get $n = 1 + \frac{3A_1R^2}{a^2Re^2}$, which upon non-dimensionalizing gives Equation (5)[1,3].

$$n = 1 + 3A_1.\tag{5}$$

3 Location of Equilibrium Points

The equations of motion (1) are found to have singular solutions at the five points[33] called the Lagrange points, liberation points or equilibrium points. Three of these equilibrium points (collinear equilibrium points - L_1, L_2 and L_3) lie on the line joining the primaries and the other two (triangular equilibrium points - L_4 and L_5) form nearly equilateral triangles[10] with the primaries. At these equilibrium points the first derivatives of the force function are zero i.e., $\Omega_x = \Omega_y = 0$[10,33].

3.1 Location of Collinear Equilibrium Points

As the collinear equilibrium points lie on the x-axis, in addition to the conditions $\Omega_x = \Omega_y = 0$, they also satisfy $y = 0$. Therefore, by equating Ω_x and y to zero and making the corresponding substitutions from Equations (6), we get the seventh degree polynomials given by Equations (7), (8) and (9) for the locations of L_1, L_2 and L_3, respectively, which upon solving with the help of MATLAB for different values of μ and A_1 gives the locations of the collinear equilibrium points.

$$x_1 = \mu - 1 - \rho_1,$$
$$x_2 = \mu - 1 + \rho_2,$$
$$x_3 = \mu + \rho_3,\tag{6}$$
$$y_1 = y_2 = y_3 = 0.$$

$$\begin{aligned}&(2+12A_1)\rho_1^7 + \left[(2+12A_1)(5-\mu)\right]\rho_1^6 + \left[(2+12A_1)(10-4\mu)\right]\rho_1^5\\&+ \left[(2+12A_1)(10-6\mu)-2\right]\rho_1^4 + \left[(2+12A_1)(5-4\mu)-4(1-\mu)\right]\rho_1^3\\&+ \left[9A_1(1-\mu)-12\mu\right]\rho_1^2 - 8\mu\rho_1 - 2\mu = 0\,,\end{aligned}\tag{7}$$

$$\begin{aligned}&(2+12A_1)\rho_2^7 - \left[(2+12A_1)(5-\mu)\right]\rho_2^6 + \left[(2+12A_1)(10-4\mu)\right]\rho_2^5\\&+ \left[(2+12A_1)(10-6\mu)-(2-4\mu)\right]\rho_2^4 + \left[(2+12A_1)(5-4\mu)-4+12\mu\right]\rho_2^3\\&+ \left[9A_1(1-\mu)-12\mu\right]\rho_2^2 + 8\mu\rho_2 - 2\mu = 0\,,\end{aligned}\tag{8}$$

$$\begin{aligned}&(2+12A_1)\rho_3^7 + \left[(2+12A_1)(2+\mu)\right]\rho_3^6 + \left[(2+12A_1)(1+2\mu)\right]\rho_3^5\\&+ \left[(2+12A_1)\mu-2\right]\rho_3^4 - 4(1-\mu)\rho_3^3 - \left[(2+3A_1)(1-\mu)\right]\rho_3^2\\&-6(1-\mu)A_1\rho_3 - 3(1-\mu)A_1 = 0\,.\end{aligned}\tag{9}$$

The location and stability of the equilibrium points are analysed for the different planetary systems given in [Table 1]. The locations of the three collinear equilibrium points for these systems with and without the oblateness coefficient A_1 and their corresponding shifts in kilometres are listed in Tables 2, 3 and 4 , respectively. The shifts in the position of the collinear equilibrium points are in a range of an order of 10^1 to 10^3 kilometres in the dimensional frame. It is interesting to note that all the three collinear points move towards the more massive primary with oblateness with the new mean motion taken in this study. Earlier in [10], with the mean motion $n^2 = 1 + 3A_1/2$ being utilized so far in the literature, it was noticed that only L_1 moves towards the barycentre. The present observation is very interesting with the new mean motion as the direction of shift of L_2 and L_3 has changed and symmetry is obtained in the shift of the collinear points. Maximum shift in Saturn – Tethys system of 226.3 km is observed. Maximum shift in Saturn – Mimas of 721.1 km is found. Maximum shift of 1151.8 km is found in L_3 for Saturn-Mimas system, whose oblateness coefficient (A_1) is maximum (0.004235) of the 11 systems chosen for the study.

Table 1. Planetary systems and their parameters

S. No.	System	μ	A_1	R (km)
1	Jupiter – Io	0.0000415283	0.0006701421	421800
2	Jupiter – Europa	0.0000250794	0.0002646382	671100
3	Jupiter – Ganymede	0.0000807835	0.0001040401	1070400
4	Jupiter – Callisto	0.0000479677	0.0000337017	1882700
5	Saturn – Mimas	0.0000000659	0.0042349996	185539
6	Saturn – Enceladus	0.0000001480	0.0025865767	238037
7	Saturn – Tethys	0.0000010950	0.0016835857	294672
8	Saturn – Dione	0.0000020390	0.0010308526	377415
9	Saturn – Rhea	0.0000032000	0.0005275432	527068
10	Saturn – Titan	0.0002461294	0.0000981153	1221865
11	Saturn – Hyperion	0.0000002000	0.0000667989	1500934

Table 2. Locations of L_1

| S. No. | x_{L_1} | | |
	with $A_1 = 0$	with $A_1 \neq 0$	Shift (km)
1	-1.0241601645	-1.0237986154	152.50141
2	-1.0204068383	-1.0202647840	95.33237
3	-1.0301894364	-1.0301312540	62.27845
4	-1.0253548320	-1.0253362861	34.91631
5	-1.0028031696	-1.0016537342	213.26510
6	-1.0036719149	-1.0027279336	224.70248
7	-1.0071624574	-1.0063945723	226.27425
8	-1.0088158731	-1.0083140311	189.40271
9	-1.0102489352	-1.0099818079	140.79427
10	-1.0438287827	-1.0436846088	176.16102
11	-1.0040600743	-1.0040264186	50.51495

Table 3. Location of L_2

S. No.	x_{L_2}		
	with $A_1 = 0$	*with* $A_1 \neq 0$	Shift (km)
1	-0.9761410952	-0.9758344587	129.33928
2	-0.9798175902	-0.9796952645	82.09280
3	-0.9702478526	-0.9702019533	49.13061
4	-0.9749723121	-0.9749571393	28.56585
5	-0.9972019276	-0.9933151479	721.14922
6	-0.9963367564	-0.9945473470	425.94563
7	-0.9928694013	-0.9919540167	269.73821
8	-0.9912315837	-0.9907059755	198.37243
9	-0.9898142613	-0.9895550788	136.60678
10	-0.9569373834	-0.9568352642	124.77587
11	-0.9959504866	-0.9959173637	49.71529

Table 4. Location of L_3

S. No.	x_{L_3}		
	with $A_1 = 0$	*with* $A_1 \neq 0$	Shift (km)
1	1.0000173034	0.9990158024	422.43312
2	1.0000104497	0.9996140741	266.00763
3	1.0000336598	0.9998776948	166.94488
4	1.0000199865	0.9999694445	95.15541
5	1.0000000275	0.9937923687	1151.76281
6	1.0000000617	0.9961746748	910.58362
7	1.0000004562	0.9974982645	737.32583
8	1.0000008496	0.9984632933	580.29681
9	1.0000013333	0.9992123096	415.86916
10	1.0001025539	0.9997339019	450.44300
11	1.0000000833	0.9998999218	150.33581

3.2 Location of Triangular Equilibrium Points

Solving the equations $\Omega_x = 0$ and $\Omega_y = 0$, the values of r_1 and r_2 are related to the mean motion values by the following equations.

$$2r_1^5 n^2 - 2r_1^2 - 3A_1 = 0,$$

$$r_2 = \eta^{-\frac{2}{3}}.$$

(10)

Substituting the mean motion value n and solving Equations (10) by series expansion method, we get the values of r_1 and r_2. The Equations (11) are obtained by truncating the higher-order terms (of orders 2 and above) of oblateness coefficient A_1. While the value of r_1 remains undisturbed by the oblateness of the more-massive primary in the CRTBP in the literature[10,14], with the new mean motion, both the values of r_1 and r_2 are affected by A_1. Also, the effect of A_1 increases in the case of r_2.

$$r_1 = 1 - \frac{3}{2}A_1,$$

$$r_2 = 1 - 2A_1.$$

(11)

Substituting these values in Equations (3) and solving for x and y, the triangular equilibrium points are located by Equations (12). These points form near-equilateral triangles[8,10] with the primaries. Equations (12) suggest that the varied mean motion

does not affect the x-location of the triangular equilibrium points [14] till linear terms of A_1, but it affects the y-location of $L_{4,5}$. However, the effect of new mean motion is noticed in the x-coordinate of the triangular points when higher order terms are taken into account. Also, when the necessary changes are made from elliptic RTBP to the CRTBP, the equations show excellent agreement with [3]. Also, [3] shows that the effect of A_1 on the location of the triangular equilibrium points is reduced by the orbital eccentricity of the primaries.

$$x = \mu - \frac{1}{2} - \frac{A_1}{2},$$

$$y = \pm \frac{\sqrt{3}}{2} \left(1 - \frac{7}{3}A_1\right). \tag{12}$$

The locations of the triangular equilibrium points for the systems in [Table 1] and their shifts due to the oblateness effect are given in [Table 5]. [Table 5] shows that the triangular equilibrium points are shifted away from the barycentre in the x-direction and that they move towards the barycentre in the y-direction. Among the shifts in the location of the equilibrium points, the shift in the y-direction of the triangular points are the maximum. They range above 200 kilometres in the dimensional coordinates for all the cases taken in [Table 1]. Maximum shifts of 392.9 km and 1587.8 km in the x and y co-ordinates, respectively, are noticed in the Saturn-Mimas system, whose oblateness coefficient A_1 is maximum of the 11 systems chosen for this study.

Table 5. Locations of the triangular equilibrium points

S. No.	x_{L_4, L_5}			y_{L_4, L_5}		
	$A_1 = 0$	$A_1 \neq 0$	Shift (km)	$A_1 = 0$	$A_1 \neq 0$	Shift (km)
1	-0.4999584717	-0.5002935428	141.33297		$\pm$0.8646712303	571.19039
2	-0.4999749206	-0.5001072397	88.79935		$\pm$0.8654906425	358.87829
3	-0.4999192165	-0.4999712366	55.68226		$\pm$0.8658151673	225.03718
4	-0.4999520323	-0.4999688832	31.72509		$\pm$0.8659573019	128.21545
5	-0.4999999341	-0.5021174339	392.87879		$\pm$0.8574676302	1587.80075
6	-0.4999998520	-0.5012931404	307.85048	$\pm$0.8660254038	$\pm$0.8607986411	1244.16289
7	-0.4999989050	-0.5008406979	248.05278		$\pm$0.8626233385	1002.49339
8	-0.4999979610	-0.5005133873	194.52962		$\pm$0.8639423332	786.18209
9	-0.4999968000	-0.5002605716	139.02557		$\pm$0.8649593836	561.86515
10	-0.4997538706	-0.4998029283	59.94183		$\pm$0.8658271397	242.25200
11	-0.4999998000	-0.5000331995	50.13037		$\pm$0.8658904215	202.59948

4 Stability of Equilibrium Points

Representing the location of equilibrium points by $L_i(a,b)$, the motion near the equilibrium points can be approximated using the equations $x = a + \xi$ and $y = b + \eta$ [8,10]. The variational equations of motion for (ξ, η) in the linear analysis from Equations (1) are obtained as

$$\xi'' - 2n\eta' = \Omega_{xx}(a,b)\xi + \Omega_{xy}(a,b)\eta,$$
$$\eta'' + 2n\xi' = \Omega_{xy}(a,b)\xi + \Omega_{yy}(a,b)\eta. \tag{13}$$

Its characteristic equation and general solution are given by Equations (14) and (16), respectively [8,10]. These equations are used to study the linear stability of the equilibrium points. The points are said to be stable if any disturbance is nullified over time without causing a permanent change in the location of the points [18].

$$\lambda^4 + (\sigma_1)\lambda^2 + (\sigma_2) = 0, \tag{14}$$

$$\Lambda^2 + (\sigma_1)\Lambda + (\sigma_2) = 0,$$
$$\sigma_1 = \left(4n^2 - \Omega_{xx} - \Omega_{yy}\right) \tag{15}$$

$$\sigma_2 = \left(\Omega_{xx}\Omega_{yy} - \Omega_{xy}^2\right),$$

$$\xi = \sum_{i=1}^{4} \alpha_i e^{\lambda_i t},$$

$$\eta = \sum_{i=1}^{4} \beta_i e^{\lambda_i t}. \tag{16}$$

4.1 Stability of Collinear Equilibrium Points

At the collinear points, we have

$$\Omega_{xx} = n^2 + \frac{2(1-\mu)}{r_1^3} + \frac{2\mu}{r_2^3} + \frac{6(1-\mu)A_1}{r_1^5} > 0 \,,$$

$$\Omega_{xy} = 0 \,, \tag{17}$$

$$\Omega_{yy} = n^2 - \frac{(1-\mu)}{r_1^3} - \frac{\mu}{r_2^3} - \frac{3A_1(1-\mu)}{2r_1^5}.$$

It can be seen that $\Omega_{xx} > 0$, $\Omega_{xy} = 0$, $\Omega_{yy} < 0$. This results in $\sigma_2 < 0$. The roots of Equations (13) are

$$\lambda_{1,2} = \pm v_1 = \pm \sqrt{\frac{-\sigma_1 + \sqrt{\sigma_1^2 - 4\sigma_2}}{2}} \,,$$

$$\lambda_{3,4} = \pm i v_2 = \pm \sqrt{\frac{-\sigma_1 - \sqrt{\sigma_1^2 - 4\sigma_2}}{2}} \,. \tag{17}$$

where, the first two roots are real and the other two are imaginary. This proves that the collinear points are unstable [10,13,15]. But, if the initial conditions (ξ_0, η_0) of Equations (16) are chosen such that the values of α_1, α_2 are zero, we can generate periodic elliptic orbits around the collinear equilibrium points [10]. These elliptic orbits are centred around the collinear points with their semi-major and semi-minor axes parallel to the y- and x-axes, respectively. The orbit's eccentricity e_o and semi-major axis a_o are given by Equations (18) [1,10].

$$e_o = \sqrt{1 - \frac{1}{\sigma_3^2}}, \quad a_o = \sqrt{\sigma_3^2 a^2 + b^2}. \tag{18}$$
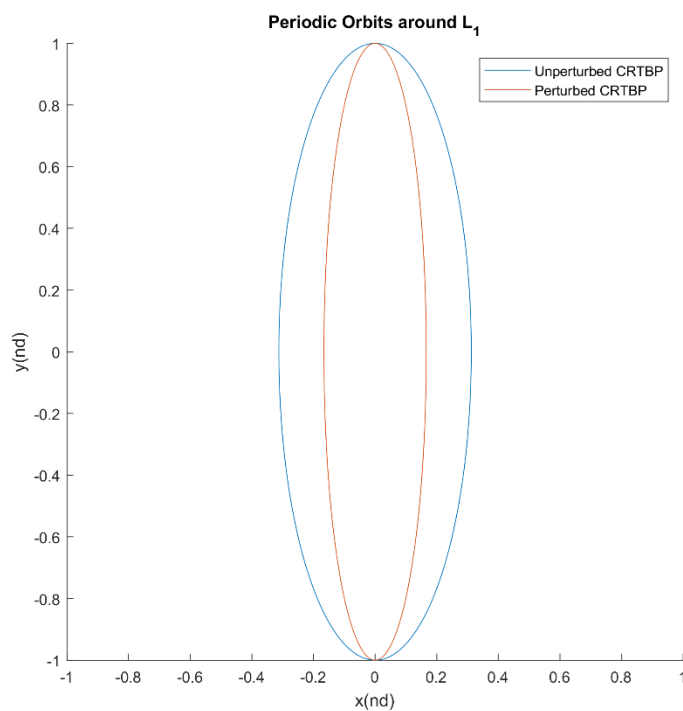
where

$$\sigma_3 = \frac{v_2^2 + \Omega_{xx}}{2v_2}. \tag{19}$$

[Table 6] lists the eccentricity of the periodic orbits around L_1, L_2 and L_3 for the systems in [Table 1]. The eccentricities of the system are affected by the oblateness of the more massive primary. Eccentricities of the orbits around L_1 and L_3 increase with the addition of oblateness [10], whereas the eccentricities of the orbits around L_2 decrease due to the change in the mean motion instead of an increase observed in [10]. There is significant decrease in eccentricity for the orbit around L$_2$ in Saturn-Mimas system from 0.95036 to 0.87558. This is again proved by the plots Figures 2, 3 and 4 . To show the effect of A_1 on the eccentricity e_o, the orbits around L_1, L_2 and L_3 in the non-dimensional frame for the Saturn-Mimas system (with highest A_1 value) in [Table 1] are plotted in Figures 2, 3 and 4 respectively, with an unchanged semi-major axis value.

Table 6. Eccentricities of the periodic orbits near the collinear Lagrangian points

| S.No. | Eccentricity | | | | | |
| | L_1 | | L_2 | | L_3 | |
	$A_1 = 0$	$A_1 \neq 0$	$A_1 = 0$	$A_1 \neq 0$	$A_1 = 0$	$A_1 \neq 0$
1	0.9485726180	0.949983158	0.9517748579	0.9504026696	0.8660254044	0.866315809
2	0.9488207988	0.949483051	0.9515277322	0.9508874119	0.8660254040	0.866140029
3	0.9481740739	0.948353168	0.9521709192	0.9520031906	0.8660254059	0.866070457
4	0.9484936280	0.948562395	0.9518534081	0.9517884343	0.8660254045	0.866039997
5	0.9499881584	0.985790165	0.9503617692	0.8755885755	0.8660254038	0.867869261
6	0.9499303335	0.974203452	0.9504195923	0.9073909887	0.8660254038	0.867149122
7	0.9496983011	0.960152007	0.9506516499	0.9377346474	0.8660254038	0.866755971
8	0.9495885513	0.955148141	0.9507614127	0.9446457582	0.8660254038	0.866472355
9	0.9494935059	0.952034416	0.9508564709	0.9482440412	0.8660254038	0.866253987
10	0.9472712881	0.947602961	0.9530631126	0.9528248103	0.8660254238	0.866068146
11	0.9499045071	0.950725478	0.9504454252	0.9496186425	0.8660254038	0.866054331

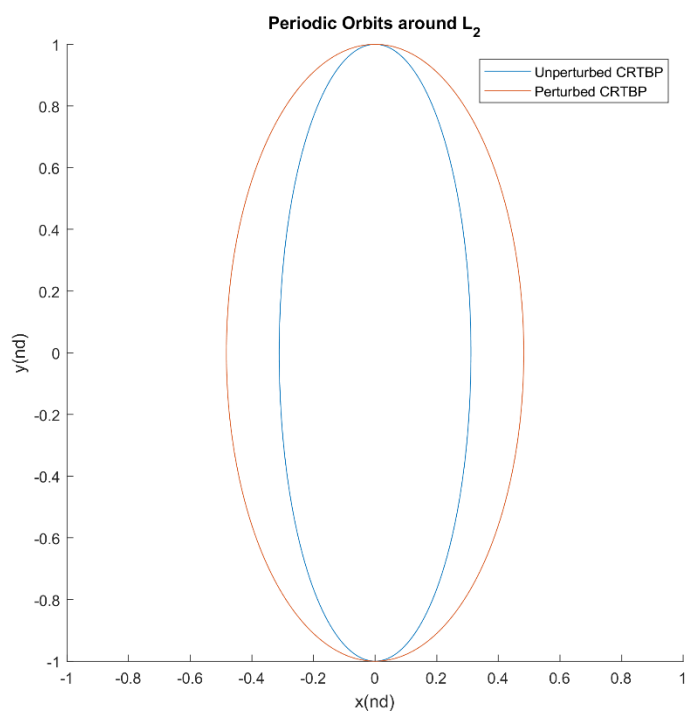**Fig 2.** Periodic orbits around the collinear equilibrium point L_1

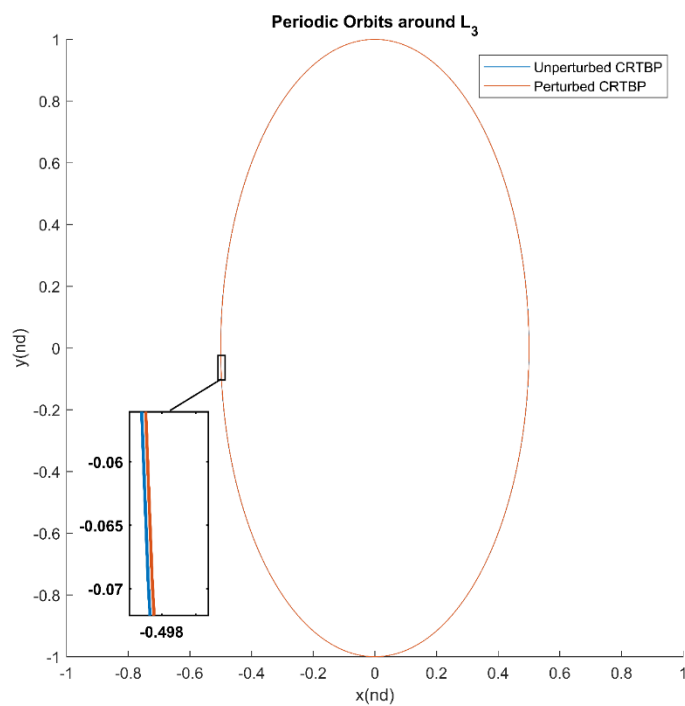**Fig 3.** Periodic orbits around the collinear equilibrium point L_2

Fig 4. Periodic orbits around collinear equilibrium point L_3

4.2 Stability of Triangular Equilibrium Points

4.2.1 Critical mass ratio

At the triangular points L_4 and L_5, we have

$$\Omega_{xx} = (x-\mu)f + (x+1-\mu)g > 0,$$
$$\Omega_{xy} = \pm y[f(x-\mu) + g(x+1-\mu)],$$
$$\Omega_{yy} = y^2(f+g) > 0,$$

where

$$f = 3(1-\mu)/r_1^5 + 15A_1/2r_1^7 > 0, g = 3\mu/r_2^5 > 0.$$

Substituting the values of r_1 and r_2 in the above equations from (11) at L_4, we get

$$\Omega_{xx} = \frac{3}{4} + 9A_1 - 3\mu A_1,$$

$$\Omega_{yy} = \frac{9}{4} + 12A_1, \tag{20}$$

$$\Omega_{xy} = \frac{\sqrt{3}}{2}\left(3\mu - \frac{3}{2} + 23\mu A_1 - 13A_1\right).$$

The roots of the characteristic Equations (14) are

$$\Lambda_{1,2} = \sqrt{\frac{-\sigma_1 \pm \sqrt{\sigma_1^2 - 4\sigma_2}}{2}}. \tag{21}$$

where, $D = \sigma_1^2 - 4\sigma_2$. As given by[33], for the triangular equilibrium points to be stable, the discriminant D of Equation (14) should be zero. Therefore, $\sigma_1^2 - 4\sigma_2 = 0$. Applying this condition results in Equation (22) which enables in finding a limiting value for the mass ratio, called the critical mass ratio μ_c, within which the system will be linearly stable.

$$1 - 6A_1 + (-27 - 84A_1)\mu_c + (27 + 90A_1)\mu_c^2 = 0. \tag{22}$$

Solving Equation (22) and truncating the higher order terms of A_1, the critical mass ratio is

$$\mu_c = \frac{1}{2}\left(1 - \frac{\sqrt{69}}{9}\right) - \frac{1}{9}\left(1 + \frac{19}{\sqrt{69}}\right)A_1, \tag{23}$$

$$\mu_c = \mu_0 - 0.3652590232\,A_1. \tag{24}$$

With $n^2 = 1 + 3\,A_1/2$, we have from[8],

$$\mu_c = \frac{1}{2}\left(1 - \frac{\sqrt{69}}{9}\right) - \frac{1}{9}\left(1 + \frac{13}{\sqrt{69}}\right)A_1, \tag{25}$$

$$\mu_c = \mu_0 - 0.28500179A_1. \tag{26}$$

Here μ_0 is the critical mass ratio for the unperturbed CRTBP which is equal to 0.038520896505[33]. From equations (24) and (26) we prove that the critical mass ratio μ_c further decreases with the new mean motion value. It is inferred from[4] that the value of μ_c increases with the oblateness of the smaller primary. It may be pointed out that the critical mass ratio μ_c in Equations (23) and (24) agrees as a particular case with that of[3], after making appropriate changes to convert the ERTBP to CRTBP.

From Equations (23) to (26), it can be seen that with the coefficient of A_1 increase in the new mean motion expression, the critical mass ratio μ_c further decreases[8,14], where the mean motion value is $n^2 = 1 + 3\frac{A1}{2}$. [Table 7] lists the critical mass ratio values for different oblateness coefficients from[8] and with Equation (23), which clearly depicts further reduction in the critical mass ratio μ_c with the current mean motion.

Table 7. Variation of critical mass ratio with A_1

A_1	$\mu_c{}^{(8)}$	μ_c
0.100000	0.010020717725	0.001994994186
0.050000	0.024270807115	0.020257945345
0.010000	0.035670878627	0.034868306273
0.005000	0.037095887866	0.036694601389
0.001000	0.038235894717	0.038155637481
0.000500	0.038378395611	0.038338266993
0.000100	0.038492396326	0.038484370602
0.000050	0.038506646415	0.038502633553
0.000010	0.038518046487	0.038517243914
0.000005	0.038519471496	0.038519070209
0.000001	0.038520611503	0.038520531246

4.2.2 Long- and short- periodic terms when the discriminant is greater than zero

When $0 < \mu \leq \mu_c$, the discriminant D of Equation (21) is greater than zero. This gives a linearly stable solution of the characteristic equation for the triangular points with long- and short-periodic terms[10,11] given by Equations (27).

$$\lambda_{1,2} = \pm i(-\Lambda_1)^{\frac{1}{2}} = \pm is_4,$$

$$\lambda_{3,4} = \pm i(-\Lambda_2)^{\frac{1}{2}} = \pm is_5. \tag{27}$$

The series expansions restricting to A_1 terms of s_4 and s_5 with the oblateness of the more massive primary are:

$$s_4 = \frac{3\sqrt{3}\sqrt{\mu}}{2}\Big[1 + \frac{23}{8}\mu + \frac{4439}{128}\mu^2 + \frac{548711}{1024}\mu^3 + O(\mu^4)$$
$$+ A_1\left(\frac{37}{6} + \frac{2291}{48}\mu + \frac{680627}{768}\mu^2 + \frac{114994403}{6144}\mu^3 + O(\mu^4)\right)\Big]$$

$$s_5 = 1 - \frac{27}{8}\mu - \frac{3213}{128}\mu^2 - \frac{355023}{1024}\mu^3 + O(\mu^4)$$
$$- A_1\left(-\frac{3}{2} + \frac{561}{16}\mu + \frac{133767}{256}\mu^2 + \frac{21453741}{2048}\mu^3 + O(\mu^4)\right) \tag{28}$$

From Equations (28), it is obvious that the long-period frequency (s_4) increases with oblateness and a further increase is observed when comparing the series expansion of s_4 with that of[11]. Similarly, truncating the higher order terms, the short-period frequency(s_5) decreases with A_1 when $\mu > 0.0266053866$. The variation of s_4 and s_5 with A_1 are tabulated in [Table 8].

Table 8. Angular Frequencies - $L_{4,5}$

S. No.	s_4		s_5		s_z
	$A_1 = 0$	$A_1 \neq 0$	$A_1 = 0$	$A_1 \neq 0$	
1	0.0167446409	0.0168435533	0.9998597987	1.0008630298	1.0030110645
2	0.0130119318	0.0130391763	0.9999153412	1.0003119086	1.0011901537
3	0.0233568446	0.0233723479	0.9997271917	0.9998829326	1.0004680583
4	0.0179964257	0.0180002369	0.9998380512	0.9998885445	1.0001516437
5	0.0006669521	0.0063495951	0.9999997776	1.0063124178	1.0188792841
6	0.0009995003	0.0039960385	0.9999995005	1.0038644146	1.0115726317
7	0.0027186939	0.0037268803	0.9999963043	1.0025152732	1.0075476494
8	0.0037099072	0.0040399936	0.9999931183	1.0015369402	1.0046281238

Continued on next page

Table 8 continued

9	0.0046476228	0.0047292641	0.9999891997	1.0007798303	1.0023711307
10	0.0407888777	0.0408138380	0.9991677874	0.9993140892	1.0004413852
11	0.0011618957	0.0011666839	0.9999993250	1.0000995128	1.0003005499

This solution results in a retrograde periodic elliptic motion [12] which is inclined at an angle α, a function of the second derivatives. From [12], the relation between α and the second derivatives is given by

$$\alpha = \frac{1}{2} tan^{-1} \left[\frac{2\Omega_{xy}}{\Omega_{xx} - \Omega_{yy}} \right], \tag{29}$$

When the mean motion is $n^2 = 1 + \frac{3}{2}A_1$,

$$tan2\alpha = \sqrt{3} - 2\sqrt{3}\mu + A_1 \left(\frac{8}{\sqrt{3}} - \frac{16}{\sqrt{3}}\mu + 4\sqrt{3}\mu^2 \right). \tag{30}$$

When the mean motion is $n^2 = 1 + 6A_1$ (the current study),

$$tan2\alpha = \sqrt{3} - 2\sqrt{3}\mu + A_1 \left(\frac{20}{\sqrt{3}} - \frac{40}{\sqrt{3}}\mu + 4\sqrt{3}\mu^2 \right). \tag{31}$$

It is clearly seen from Equations (30) and (31) that the angle α increases with A_1 and that this increase is further enhanced with the inclusion of the new mean motion expression.

4.2.3 Secular solutions when the discriminant is equal to zero

When the discriminant is negative, the roots of Equations (14) will give a complex value with non-zero real and imaginary parts resulting in an unstable solution. But, we get purely imaginary roots [Equations (32)] when the discriminant $D = 0$.

$$\lambda_{1,3} = ik^{\frac{1}{2}}, \quad \lambda_{2,4} = -ik^{\frac{1}{2}}, \tag{32}$$

$$k = \frac{\sigma_1}{2} > 0. \tag{33}$$

However, elliptic retrograde orbits can be established if the initial coordinates are combined with special velocity components. Transforming the coordinates at the triangular points about an angle α *given by* (29):

$$\xi = \bar{\xi} cos\alpha - \bar{\eta} sin\alpha,$$

$$\eta = \bar{\xi} sin\alpha + \bar{\eta} cos\alpha. \tag{34}$$

Substituting the above equation in Equations (13), we get

$$\bar{\xi}'' - 2n\bar{\eta}' = \lambda_2^* \bar{\xi},$$

$$\eta'' + 2n\bar{\xi}' = \lambda_1^* \bar{\eta}, \tag{35}$$

where

$$\bar{\lambda}_{1,2}^* = \left(2n^2 - k \right) \pm 2n\sqrt{n^2 - k}. \tag{36}$$

Solving Equations (34), using Laplace transformation, the solutions can be written[12] in terms of the initial position and velocities $(\bar{\xi}_0, \bar{\eta}_0, \bar{\xi}_0{}', \bar{\eta}_0{}')$ as

$$\bar{\xi} = \left[\bar{\xi}_0 + \left\{\frac{\left(k+\overline{\lambda_1^*}\right)\bar{\xi}_0{}'}{2k} - \frac{n\overline{\lambda_1^*}\,\overline{\eta}_0}{k}\right\}t\right]\cos\sqrt{k}t$$

$$+ \left[\left\{\frac{n\overline{\lambda_1^*}\,\overline{\eta}_0}{k^{\frac{3}{2}}} - \frac{\left(\overline{\lambda_1^*}-k\right)\bar{\xi}_0{}'}{2k^{\frac{3}{2}}}\right\} + \left\{\frac{\left(k+\overline{\lambda_2^*}\right)\bar{\xi}_0}{2k^{\frac{1}{2}}} + \frac{n\overline{\eta}_0{}'}{k^{\frac{1}{2}}}\right\}t\right]\sin\sqrt{k}t, \tag{37}$$

$$\bar{\eta} = \left[\bar{\eta}_0 + \left\{\frac{\left(k+\overline{\lambda_2^*}\right)\bar{\eta}_0{}'}{2k} - \frac{n\overline{\lambda_2^*}\,\bar{\xi}_0}{k}\right\}t\right]\cos\sqrt{k}t$$

$$+ \left[\left\{\frac{\left(k-\overline{\lambda_2^*}\right)\bar{\eta}_0{}'}{2k^{\frac{3}{2}}} - \frac{n\overline{\lambda_2^*}}{k^{\frac{3}{2}}}\right\}\bar{\xi}_0 + \left\{\frac{\left(k+\overline{\lambda_1^*}\right)\bar{\eta}_0}{2k^{\frac{1}{2}}} - \frac{n\bar{\xi}_0{}'}{k^{\frac{1}{2}}}\right\}t\right]\sin\sqrt{k}t.$$

It is clear that, in this case also, due to the secular terms in t, the solution is unstable[12]. However, retrograde elliptic periodic orbits can be shown when the initial conditions are combined with special velocity components as

$$\bar{\xi}_0{}' = \frac{\sqrt{k}\bar{\eta}_0}{m}, \quad \bar{\eta}_0{}' = -\sqrt{k}m\bar{\xi}_0. \tag{38}$$

where

$$m = \sqrt{\frac{\left(k+\overline{\lambda_2^*}\right)}{\left(k+\overline{\lambda_1^*}\right)}}. \tag{39}$$

Eliminating the secular terms from Equations (37), we get

$$\bar{\xi} = \bar{\xi}_0\cos\sqrt{k}t + \frac{\bar{\eta}_0}{m}\sin\sqrt{k}t, \tag{40}$$

$$\bar{\eta} = \bar{\eta}_0\cos\sqrt{k}t - m\bar{\xi}_0\sin\sqrt{k}t.$$

Further eliminating t from the above equations, we have

$$m^2\bar{\xi}^2 + \bar{\eta}^2 = m^2\bar{\xi}_0^2 + \bar{\eta}_0^2. \tag{41}$$

Equations (41) represents an ellipse with eccentricity $e = \sqrt{1-m^2}$, which after some algebra is equal to

$$e = \sqrt{2(\sqrt{2}-1)}\left[1 - \frac{3\left(2-\sqrt{2}\right)}{4}A_1\left(\mu-1\right)\right]. \tag{42}$$

It can be seen that the eccentricity exactly matches with the result of[12] till the first power of A_1. However, we have noticed that when the higher order terms of A_1 are included, the eccentricity shows a further increase. At $\left(\bar{\xi}_0, 0\right)$, the velocity components from Equations (38) become

$$\bar{\xi}_0{}' = 0, \ \bar{\eta}_0{}' = -\sqrt{km}\bar{\xi}_0. \tag{43}$$

As $\sqrt{km}$ is always positive, $\bar{\eta}_0{}'$ always gets a sign opposite to that of $\bar{\xi}_0$. This shows that the periodic orbits represented by Equations (40) are retrograde.

5 Tadpole Orbits around Triangular Equilibrium points

For small distances from the triangular equilibrium points, trajectories in the synodic frame can be obtained by integrating the variational equations of motion. This way, we obtain particle paths, a combination of the short- and long-periodic orbits called the Tadpole orbits[35] starting very close to the triangular points. These tadpole orbits define the movement of Trojan bodies around L_4 and L_5 points of the Sun-Jupiter system[35]. The Trojan orbits can be approximated by using the Tadpole orbits with suitable perturbations in the Restricted Three–Body Problem[36].

With the help of the second derivatives of the force function $(\Omega_{xx}, \Omega_{xy}, \Omega_{yy})$ at the triangular equilibrium points, the roots of Equations (14) are expressed as

$$\lambda_{1,2} = \pm i v_1 = \pm \sqrt{\frac{-\sigma_1 + \sqrt{\sigma_1^2 - 4\sigma_2}}{2}},$$

$$\lambda_{3,4} = \pm i v_2 = \pm \sqrt{\frac{-\sigma_1 - \sqrt{\sigma_1^2 - 4\sigma_2}}{2}}. \tag{44}$$

Here, all the four roots of the system are found to be imaginary, if the value of the mass ratio μ of the system lies within the range $0 < \mu < \mu_c$[33]. This, in turn makes the equilibrium points L_4 and L_5 stable[33,37]. In Equations (44), $v_{1,2}$ are the frequencies of the long- and short-periodic orbits. As all of the roots are proved to be imaginary, we can write the solution of Equations (14) to be

$$\xi(f) = \alpha_1 \cos(v_1 f) + \alpha_2 \sin(v_1 f) + \alpha_3 \cos(v_2 f) + \alpha_4 \sin(v_2 f),$$

$$\eta(f) = \beta_1 \cos(v_1 f) + \beta_2 \sin(v_1 f) + \beta_3 \cos(v_2 f) + \beta_4 \sin(v_2 f) \tag{45}$$

We have chosen the Saturn-Titan system ($\mu = 0.0002461294, A_1 = 0.0000981153$) to examine the Tadpole orbits under the CRTBP with the oblateness of the more massive primary and to understand the effect of A_1 on the tadpole orbits. The initial conditions[21] of Equations (45) are $\xi_0 = \xi(0) = \alpha_1 + \alpha_3, \xi_0' = \xi'(0) = \alpha_4 v_2 + \alpha_2 v_1, \eta_0 = \eta(0) = \beta_1 + \beta_3, \eta_0' = \eta'(0) = \beta_4 v_2 + \beta_2 v_1$. The coefficients are related to each other[21] as:

$$\alpha_1 = -\frac{2\beta_2 v_1 + \Omega_{xy}\beta_1}{v_1^2 + \Omega_{xx}}, \quad \alpha_2 = \frac{2\beta_1 v_1 - \Omega_{xy}\beta_2}{v_1^2 + \Omega_{xx}}$$

$$\alpha_3 = \frac{-2\beta_4 v_2 - \Omega_{xy}\beta_3}{v_2^2 + \Omega_{xx}}, \quad \alpha_4 = \frac{2\beta_3 v_2 - \Omega_{xy}\beta_4}{v_2^2 + \Omega_{xx}}$$

$$\beta_1 = \frac{2\alpha_2 v_1 - xy\alpha_1}{v_1^2 + \Omega_{yy}}, \quad \beta_2 = -\frac{2\alpha_1 v_1 + \Omega_{xy}\alpha_2}{v_1^2 + \Omega_{yy}}$$

$$\beta_3 = \frac{2\alpha_4 v_2 - \Omega_{xy}\alpha_3}{v_2^2 + \Omega_{yy}}, \quad \beta_4 = -\frac{2\alpha_3 v_2 + \Omega_{xy}\alpha_4}{v_2^2 + \Omega_{yy}}.$$

The initial conditions for the current case (sample orbits) are chosen to be $\xi_0 = 0.0001, \xi_0' = 0.005, \eta_0 = 0.0001, \eta'(0) = 0.005$ and the system of equations are solved using MATLAB to get the coefficients $\alpha_1, \alpha_2, \alpha_3, \alpha_4$ and $\beta_1, \beta_2, \beta_3, \beta_4$ of the Equations (45). Among these coefficients, $\alpha_1, \alpha_2, \beta_1, \beta_2$ correspond to the long-periodic orbit and $\alpha_3, \alpha_4, \beta_3, \beta_4$ correspond to the short-periodic orbit.

[Figure 6] shows the long- and short-periodic orbits of the Saturn-Titan System. The periodic eccentricity and the semi-major axis of the long- and short-periodic orbits can be calculated by using the Equations (18) and (19). The eccentricity and the semi-major axis of the long-periodic orbit are 0.9943196 and 9.448440e-04, respectively in the non-dimensional frame when $A_1 = 0$. When A_1 is included, both the values increase and become 0.99432100 and 9.4495728e-04, respectively. Considering the short-periodic orbit, the eccentricity decreases from 0.5535525 to 0.5533317 and the semi-major axis increases from 1.3287025e-04 to 1.3287564e-04 by taking A_1 into account. [Figure 5] gives the combined long- and short-period, the Tadpole orbit plotted for the Saturn-Titan system for 400 Earth days. The tadpole orbit is affected by A_1 and shows a shift of up to 100 km in its trajectory in the dimensional frame.

Figures 7 and 8 shows the frequencies of the Tadpole orbits. It is clearly seen that the values locally repeat with a time period given by the short-period over a mean line which tends to vary with a frequency of the long-period. The orbital frequency of the long- and short-periodic orbits are 0.0399984 and 0.9991997, respectively, in the unperturbed CRTBP. When oblateness effect is included, the frequency of the long-periodic orbit increases to 0.0400031 and that of the short-periodic orbit decreases to 0.9991400. Therefore, when $A_1 \neq 0$, time period of the long-periodic orbit (T_1) decreases and that of the short periodic orbit (T_2) increases. In the synodic system, the orbital period of the long- and short-periodic orbits are 157.0676 and 6.2886, respectively. The orbital period of Titan around Saturn is 15.945 Earth days. Taking that into account and converting the synodic system into dimensional coordinates, the long-period of the Tadpole orbit is 398.5944 Earth days and the short-period is 15.9587 Earth days.
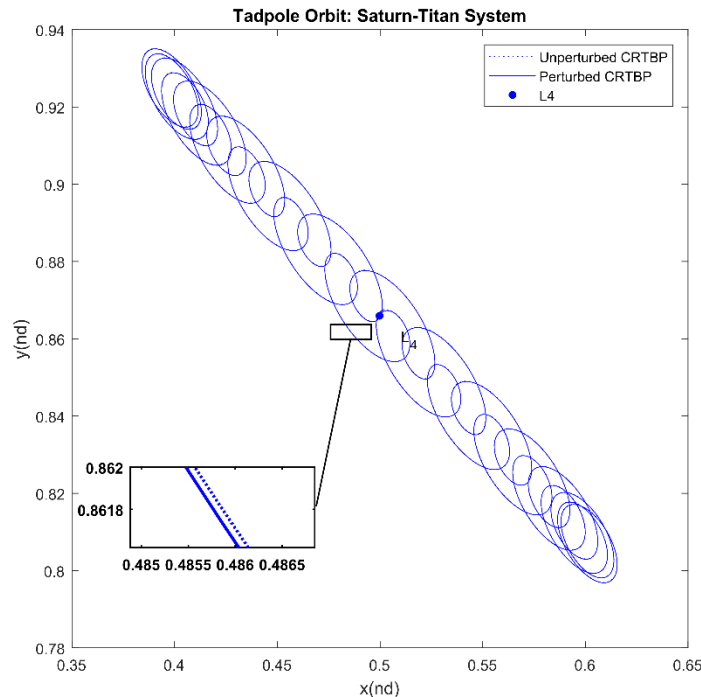

Fig 5. Tadpole orbit around triangular equilibrium point L_4 in Saturn-Titan System for 400 Earth days
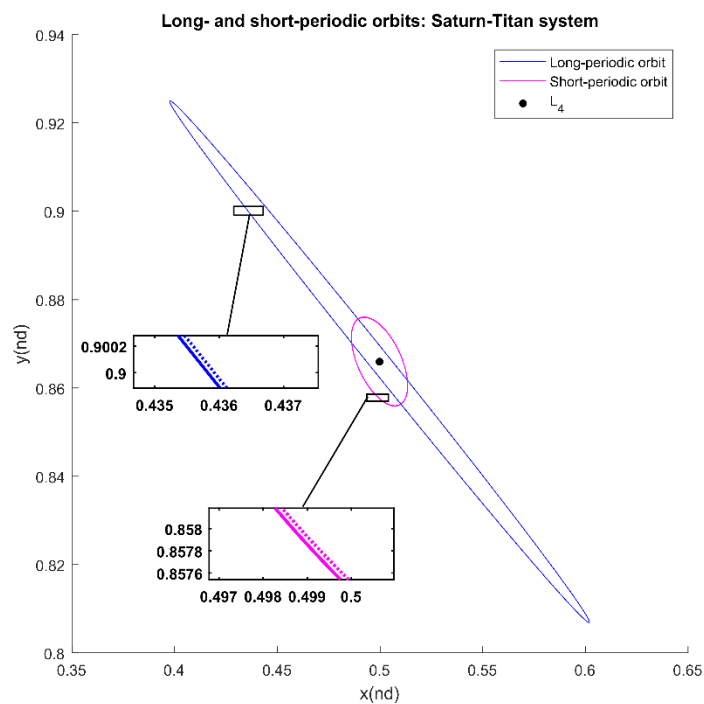
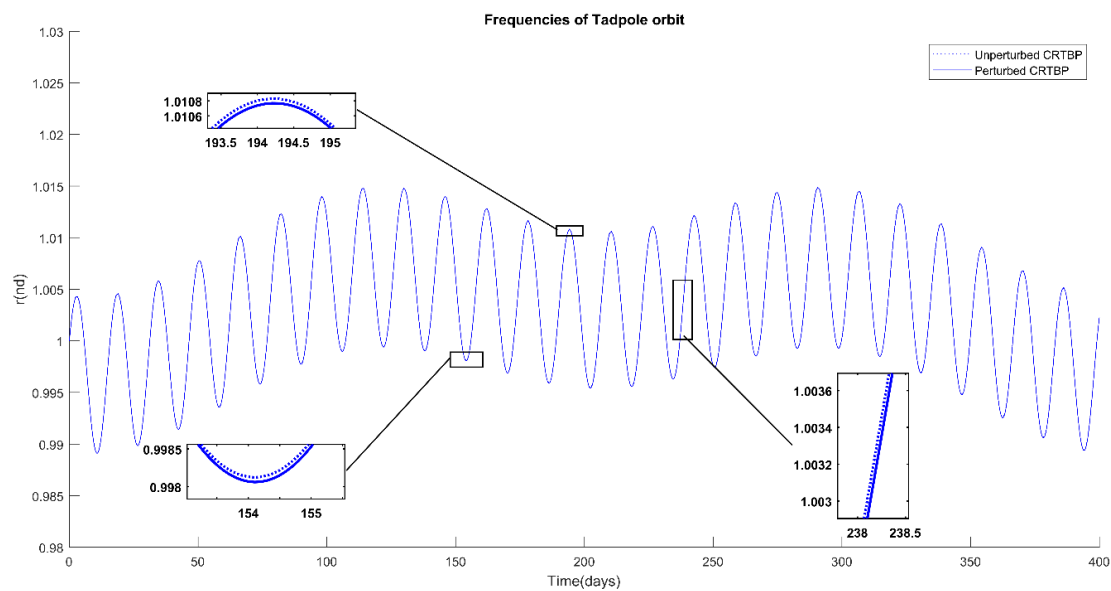**Fig 6.** Long- and short-periodic orbits of Tadpole orbits (Saturn-Titan system)
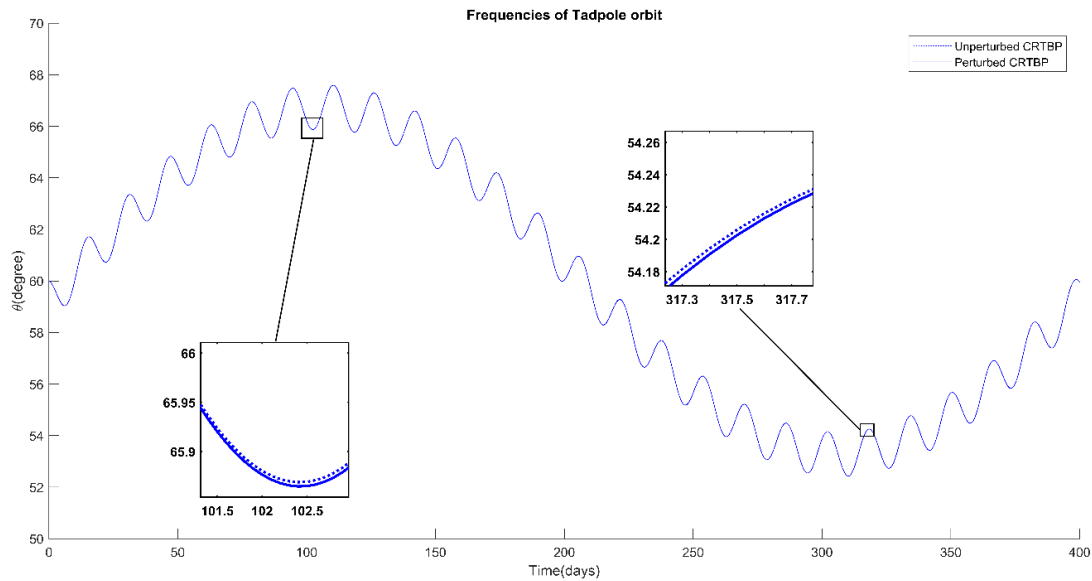

Fig 7. Frequencies of the Tadpole Orbits (position)

Fig 8. Frequencies of the Tadpole Orbits (true anomaly)

6 Three-Dimensional Case

The equations of motion in the three-dimensional case are[10]

$$x'' - 2ny' = \Omega_x,$$

$$y'' + 2nx' = \Omega_y, \tag{46}$$

$$z'' = \Omega_z,$$

where

$$\Omega = \frac{n^2}{2}\left(x^2 + y^2\right) + \left[\frac{1-\mu}{r_1} + \frac{\mu}{r_2} + \frac{(1-\mu)A_1}{2r_1^3} - \frac{3(1-\mu)A_1 z^2}{2r_1^5}\right]. \tag{47}$$

With

$$r_1^2 = (x-\mu)^2 + y^2 + z^2,$$
$$r_2^2 = (x+1-\mu)^2 + y^2 + z^2. \tag{48}$$

Similar to the planar RTBP, in the three-dimensional case also, the singularities are obtained by equating x', y', z' and hence $\Omega_x, \Omega_y, \Omega_z$ to zero. It can be proved that the system gets five equilibrium points in the xy-plane and the points are located in the same places as in the planar case[10]. At the equilibrium points, $\Omega_{xz} = \Omega_{yz} = 0$, hence, the variational equations are given by[10]

$$\xi'' - 2n\eta' = \Omega_{xx}(a,b,c)\xi + \Omega_{xy}(a,b,c)\eta,$$

$$\eta'' + 2n\xi' = \Omega_{xy}(a,b,c)\xi + \Omega_{yy}(a,b,c)\eta, \tag{49}$$

$$\zeta'' = \Omega_{zz}(a,b,c)\zeta.$$

where, $x = a + \xi$, $y = b + \eta$, $z = c + \zeta$. The second derivatives are to be evaluated at the equilibrium points. The motion, therefore, in the xy-plane does not influence the motion in the z-direction at the five equilibrium points. The mean in the z-direction is also affected by the second derivatives, whose relation at the collinear points is

$\Omega_{xx} + \Omega_{yy} + \Omega_{zz} = 2n^2$.

The mean motion in the z-direction is

$$s_z = \sqrt{-\Omega_{zz}} = \sqrt{\Omega_{xx} + \Omega_{yy} - 2n^2}, \tag{50}$$

$$s_z = 1 + \frac{3A_1}{2}(3 - \mu) > n. \tag{51}$$

$$s_z = 1 + \frac{3A_1}{2}(3/2 - \mu) > n. \tag{52}$$

Equation (50) gives the angular velocities s_z for the triangular points $L_{4,5}$. This value is always greater than the mean motion of the primaries[10] as observed from [Table 8] and Equation (51). Equation (52) provides s_z when the mean motion is $n^2 = 1 + 3A_1/2$. From Equations (51) and (52), we easily notice that s_z increases further with the new mean motion. This result will play an important role in studying three-dimensional periodic orbits around the triangular points with oblateness.

7 Results

The oblateness of the more massive primary is known to increase the mean motion of the primaries. With the secular perturbations included on argument of perigee (ω) and right ascension of ascending node (Ω) in the expression of mean motion, it is seen to further increase. With the new mean motion expression, the locations of the five equilibrium points of the circular restricted three-body problem are studied. The collinear equilibrium points move towards the more massive primary for all the three points, which is a new result. As opposed to this, the triangular points shift away from the origin in the x-direction due to oblateness. And, the x-location of the triangular points are found to be unaffected by the change in mean motion. However, the y-location is significantly affected by the change in mean motion. The points shift towards the origin in the y-direction and decrease by a high coefficient in the linear term of A_1. In the stability of the collinear points, the effect of oblateness on the eccentricities of the periodic elliptic orbits around the collinear points in conditional stability is changed by the new mean motion expression. The eccentricities for the points L_1 and L_3 increase but that for L_2 is decreases by the changed mean motion. This is a new result. The critical mass ratio for the triangular points are obtained. The critical mass ratio shows a further significant decrease due to the oblateness with new mean motion. Stability of the triangular equilibrium points for various cases of astronomical interest are studied. Series expansion of the angular frequencies till the linear terms suggest that both s_4 and s_5 increase with oblateness. s_4 shows further increase in its value due to new mean motion. The eccentricities of the retrograde periodic orbits around $L_{4,5}$ when $\mu = \mu_c$ are found. Till linear terms of A_1, the eccentricity is not affected by the change in mean motion; but an increase is observed when higher order terms in A_1 are considered. The tadpole orbits of the Saturn-Titan system get an increase in their time period of the short-periodic orbit and a decrease in the period of the long-periodic orbit. The study about the three-dimensional case of the equilibrium points brings out that the mean motion s_z of triangular points in the z-direction increases further significantly with the new mean motion.

8 Conclusion

The CRTBP with the more massive primary as an oblate spheroid with its equatorial plane coincident with the plane of motion is studied. A new mean motion expression for this study is used which is obtained by using the secular perturbation effects of oblateness of the more massive primary on the mean anomaly, argument of perigee and the right ascension of the ascending node[1]. This increases the value of mean motion of the primaries. With this mean motion value, the locations of the five equilibrium points in the planar problem are found. The shifts in their locations due to the oblateness effect are studied. It is interesting to note that all the three collinear points move towards the more massive primary with oblateness. It is a new result. Among the shifts in the collinear points, L_3 shows the highest shift towards the more massive primary. And, when the shifts of all five equilibrium points are compared, the y-coordinate of the triangular point is the highest. The linear stability of the collinear equilibrium points is studied. It is very interesting to note that the eccentricities (e) of the orbits around L_1 and L_3 increase, while it decreases around L_2 with the addition of oblateness with the new mean motion. The decrease in e is significant

in Saturn-Mimas system from 0.95036 to 0.87558. For the triangular equilibrium points, the critical mass ratio μ_c within which the system remains linearly stable is calculated in terms of the oblateness coefficient. The effect of the change in mean motion value is clearly seen in the expression for critical mass ratio. μ_c further decreases significantly from $0.285\ldots A_1\ to\ 0.365\ldots A_1$ with the new mean motion. Linear stability of the triangular equilibrium points when the mass ratio is within the limit and when it equates to the critical mass ratio μ_c are studied. The periodic retrograde motion around the triangular equilibrium points in both of the cases are studied. The combined long- and short-periodic orbits around the Saturn-Titan system are studied. The study is extended to the three-dimensional case and the mean motion sz in the z-direction for the triangular points is calculated. The mean motion S_z increases significantly with the new mean motion from $9A_1/4$ to $9A_1/2$.

Acknowledgements

References

1) Sharma RK, Sellamuthu H, Jency AA. Perturbed Trojan dynamics in the solar system. In: AAS AIAA Astrodynamics Specialist Conference. 2020;p. 20–704. Available from: https://www.researchgate.net/publication/343547691.

2) Johnson A, Sharma RK. Locations of Lagrangian points and periodic orbits around triangular points in the photo gravitational elliptic restricted three-body problem with oblateness. *International Journal of Advanced Astronomy*. 2019;7:25–38. Available from: https://doi.org/10.14419/ijaa.v7i2.29377.

3) Jency AA, Sharma RK. Location and stability of the triangular Lagrange points in photo-gravitational elliptic restricted three body problem with the more massive primary as an oblate spheroid. *International Journal of Advanced Astronomy*. 2019;7(2). Available from: https://dx.doi.org/10.14419/ijaa.v7i2.29814.

4) Arohan R, Sharma RK. Periodic orbits in the planar restricted photo-gravitational problem when the smaller primary is an oblate spheroid. *Indian Journal of Science and Technology*. 2020;13(16):1630–1640. Available from: https://doi.org/10.17485/IJST/v13i16.401.

5) Sharma RK. Perturbations of Lagrangian points in the restricted three-body problem. *Indian Journal of Pure and Applied Mathematics*. 1975;6:1099–1102.

6) Sharma RK, Rao PVS. Collinear equilibria and their characteristic exponents in the restricted three-body problem when the primaries are oblate spheroids. *Celestial Mechanics*. 1975;12(2):189–201. Available from: https://dx.doi.org/10.1007/bf01230211.

7) McCuskey SW. Introduction to Celestial Mechanics. and others, editor;Addison-Wesley Publishing Company. 1963.

8) Rao PVS, Sharma RK. A note on the stability of the triangular points of equilibrium in the restricted three-body problem. *Astronomy and Astrophysics*. 1975;43:381–383. Available from: http://adsabs.harvard.edu/abs/1975A%26A....43..381S.

9) Sharma RK. Study of Periodic Orbits in Restricted Problem taking the Bigger Primary an Oblate Spheroid. Ph.D Thesis, University of Delhi. 1976.

10) Sharma RK, Rao PVS. Stationary solutions and their characteristic exponents in the restricted three-body problem when the more massive primary is an oblate spheroid. *Celestial Mechanics*. 1976;13(2):137–149. Available from: https://dx.doi.org/10.1007/bf01232721.

11) Sharma RK, Rao PVS. A case of commensurability induced by oblateness. *Celestial Mechanics*. 1978;18(2):185–194. Available from: https://dx.doi.org/10.1007/bf01228715.

12) Sharma RK, Rao PVS. Effect of oblateness on triangular solutions at critical mass. *Astrophysics and Space Science*. 1979;60(2):247–250. Available from: https://dx.doi.org/10.1007/bf00644329.

13) Sharma RK. Periodic orbits of second kind in the restricted three-body problem when the more massive primary is an oblate spheroid. *Astrophys And Space Science*. 1981;76:255–258. Available from: https://doi.org/10.1007/.

14) Sharma RK. On linear stability of triangular libration points of the photogravitational three-body problem when the more massive primary is an oblate spheroid. In: Fricke W, Teleki G, editors. Sun and Planetary System. Dordrecht, Holland. D. Reidel Publishing Co. 1982;p. 435–436. Available from: https://doi.org/10.1007/978-94-009-7846-1_114.

15) Sharma RK, Rao PVS. On finite periodic orbits around the equilateral solutions of the planar restricted three-body problem. In: Bhatnagar KB, et al., editors. International workshop on Space Dynamics and Celestial mechanics. D. Reidel Publishing Co. 1986;p. 71–85. Available from: https://doi.org/10.1007/978-94-009-4732-0_8.

16) Sharma RK. The linear stability of libration points of the photogravitational restricted three-body problem when the smaller primary is an oblate spheroid. *Astrophys Space science*. 1987;135:271–281. Available from: https://doi.org/10.1007/BF00641562.

17) Rao PVS, Sharma RK. Oblateness effect on finite periodic orbits at L4. In: and others, editor. 39th Congress of the International Astronautical Federation;vol. 300. . Available from: https://ui.adsabs.harvard.edu/#abs/1988bang.iafcU....S/abstract.

18) Sharma RK. The periodic orbits of the second kind in terms of Giacaglia's variables with oblateness. *Earth, Moon and Planets*. 1989;45:312–318. Available from: https://ui.adsabs.harvard.edu/link_gateway/1989EM&P...45..213S/doi:10.1007/BF00057744.

19) Sharma RK. Periodic orbits of third kind in the restricted three-body problem with oblateness. *Astrophys And Space Science*. 1990;166:211–218. Available from: https://doi.org/10.1007/BF01094894.

20) Rao PVS, Sharma RK. Effect of oblateness on the non-linear stability of L 4 in the restricted three-body problem. *Celestial Mechanics and Dynamical Astronomy*. 1997;65(3):291–312. Available from: https://dx.doi.org/10.1007/bf00053510.

21) Markellos VV, Papadakis KE, Perdios EA. Non-linear stability zones around triangular equilibria in the plane circular restricted three-body problem with oblateness. *Astrophysics and Space Science*. 1996;245(1):157–164. Available from: https://dx.doi.org/10.1007/bf00637811.

22) Jain S, Kumar A, Bhatnagar KB. Periodic orbits around the collinear liberation points in the restricted three body problem when the smaller primary is a triaxial rigid body: Sun-Earth case. *Bull Astr Soc India*. 2006;34:211–223. Available from: https://ui.adsabs.harvard.edu/#abs/2006BASI...34..211J/abstract.

23) Shankaran S, Sharma JP, Ishwar B. Equilibrium points in the generalised photogravitational non-planar restricted three body problem. *International Journal of Engineering, Science and Technology*. 2011;3(2):63–67. Available from: https://dx.doi.org/10.4314/ijest.v3i2.68133.

24) Beevi AS, Sharma RK. Oblateness effect of Saturn on periodic orbits in the Saturn-Titan restricted three-body problem. *Astrophysics and Space Science*. 2012;340(2):245–261. Available from: https://dx.doi.org/10.1007/s10509-012-1052-3.

25) Arredondo JA, Guo J, Stoica C, Tamayo C. On the restricted three body problem with oblate primaries. *Astrophysics and Space Science*. 2012;341(2):315–322. Available from: https://dx.doi.org/10.1007/s10509-012-1085-7.

26) Abouelmagd EI, Asiri HM, Sharaf MA. The effect of oblateness in the perturbed restricted three-body problem. *Meccanica*. 2013;48(10):2479–2490. Available from: https://dx.doi.org/10.1007/s11012-013-9762-3.

27) Tiwary RD, Kushvah BS. Computation of halo orbits in the photogravitational Sun-Earth system with oblateness. *Astrophysics and Space Science*. 2015;357(1):1–16. Available from: https://dx.doi.org/10.1007/s10509-015-2243-5.

28) Pathak N, Thomas VO. Analysis of Effect of Oblateness of Smaller Primary on the Evolution of Periodic Orbits. *International Journal of Astronomy and Astrophysics*. 2016;06(04):440–463. Available from: https://dx.doi.org/10.4236/ijaa.2016.64036.

29) Chidambararaj P, Sharma RK. Halo Orbits around Sun-Earth L1 in Photogravitational Restricted Three-Body Problem with Oblateness of Smaller Primary. *International Journal of Astronomy and Astrophysics*. 2016;06(03):293–311. Available from: https://dx.doi.org/10.4236/ijaa.2016.63025.

30) Ansari AA, Alam M. Dynamics in the circular restricted three body problem with perturbations. *International Journal of Advanced Astronomy*. 2017;5(1):19–19. Available from: https://dx.doi.org/10.14419/ijaa.v5i1.7102.

31) Beevi AS, Sharma RK. Effect of Oblateness of the More Massive Primary on Periodic Orbits in the Restricted Three-Body Problem. *Advances in Astrophysics*. 2017;2:12–24. Available from: https://dx.doi.org/10.22606/adap.2017.21003.

32) Pathak N, Thomas VO, Abouelmagd EI. The perturbed photogravitational restricted three-body problem: analysis of resonant periodic orbits. *Discrete and continuous dynamical systems: Series S*. 2019;12:849–875. Available from: https://doi.org/10.3934/dcdss.2019057.

33) Szebehely V. Theory Of Orbits. New York. Academic Press. 1967. Available from: https://doi.org/10.1007/978-3-7091-2916-6_2.

34) Danby JMA. Fundamentals of Celestial Mechanics. 2nd ed. VA, USA. Willmann-Bell, Inc. 1988.

35) Murray CD, Dermott SF. Solar System Dynamics. Cambridge. Cambridge University Press. 1999.

36) Rabe E. Determination and survey of periodic Trojan orbits in the restricted problem of three bodies. *The Astronomical Journal*. 1961;66(9):500–500. Available from: https://dx.doi.org/10.1086/108451.

37) Singh J, Ishwar B. Stability of triangular points in the generalised photogravitational restricted three body problem. *Astronomical Society of India*. 1999;27:415–424. Available from: http://adsabs.harvard.edu/abs/1999BASI...27..415S.